Porous to Non-Porous Transition in the Morphology of Metal Assisted Etched Silicon Nanowires

Olan Lotty[1], Nikolay Petkov[1], Yordan M. Georgiev[1] and *Justin D. Holmes[1,2,]

[1]*Materials Chemistry and Analysis Group, Department of Chemistry and the Tyndall National Institute, University College Cork, Ireland.* [2]*Centre for Research on Adaptive Nanostructures and Nanodevices (CRANN), Trinity College Dublin, Dublin 2, Ireland*

Abstract

A single step metal assisted etching (MAE) process, utilizing metal ion-containing HF solutions in the absence of an external oxidant, has been developed to generate heterostructured Si nanowires with controllable porous (isotropically etched) and non-porous (anisotropically etched) segments. Detailed characterisation of both the porous and non-porous sections of the Si nanowires was provided by transmission electron microscopy studies, enabling the mechanism of nanowire roughening to be ascertained. The versatility of the MAE method for producing heterostructured Si nanowires with varied and controllable textures is discussed in detail.

*To whom correspondence should be addressed. E-mail: j.holmes@ucc.ie; Tel: +353 (0)21 4903608, Fax: +353 (0)21 4274097

1. Introduction

Silicon nanowires have been successfully exploited as components in devices that include nanoelectronics, [1-6] energy storage and conversion, [7] and photovoltaics. [8-9] Many synthetic methods have been utilized to generate silicon nanowires, including laser ablation, [10-11] thermal evaporation, [12-13] chemical vapour deposition, [14-15] and supercritical fluid growth. [16-19] However, many nanowire growth strategies do not over 100 % control over crystal orientation or the vertical alignment of the nanowires produced. Metal Assisted Etching (MAE) is widely used for the synthesis of vertically aligned silicon nanowires which does not require expensive processing equipment, is scalable over large areas and can be performed at room temperature. Many MAE methodologies have been developed which can produce silicon nanowires with uniform diameters and packing densities. [20-23]

Vertically aligned Si nanowires have been used as photovoltaic devices because of their anti-reflective characteristics and solar cell efficiencies of up to 7.3 % have been reached for nanowires prepared by MAE. [24] Porous MAE Si nanowires have also been shown to be excellent candidates as thermoelectric materials as they provide an efficient phonon scattering mechanism, throughout the phonon spectrum due to their high surface roughness. [25] Porous MAE Si nanowires have also been proposed as potential platforms upon which to build sensing technology, due to their high surface areas, [26] and as lithium battery anode materials, as porous silicon nanowires can allow for mechanical strain within their many voids during lithiation. [27-28]

The most commonly used MAE fabrication strategy is a two-step approach; firstly, a catalytic metal is deposited on to a Si substrate by electroless deposition or sputtering, followed by etching of the Si by the deposited metal using a solution containing both HF and

an oxidant such as hydrogen peroxide. Recently, "barcode" Si nanowires have been reported by Chiappini *et al.* [29] whereby the porosity of Si nanowires formed by the two-step MAE process was tuned by varying the concentration of oxidant present in the etch bath. The Si nanowires that were subsequently formed alternated in areas of varying porosity along their vertical axis.

In this article, we demonstrate the synthesis of porous to non-porous heterostructured Si nanowires in a single step etch, without the introduction of an external oxidant and show that there exists a boundary condition which separates the formation of porous and non- porous segments within the nanowires. The fabrication of porous Si wires has previously been reported in a similar work by Chen *et al.* [30] but the study did not report a gradual shift from a porous to non- porous morphology in a single step etch to generate heterostructured Si nanowires. Eliminating the need for a second step, whilst still retaining control over the morphology of Si nanowires formed by MAE, is attractive from a processing and cost perspective. Our single step MAE technique for generating porous to non- porous heterostructured Si nanowires involves electroless metal deposition onto a Si substrate, in a metal ion containing HF solution. Metal deposition in this manner is a localized chemical redox process in which both anodic and cathodic processes occur simultaneously at the silicon surface. [31] The change in the morphology of the Si nanowires formed by the single step MAE from porous to non- porous can be related to the initial concentration of metal catalyst used in the etch baths. The cores of the Si nanowires generated are single crystals and the growth direction has a defined relationship with the surface orientation of the wafer used. [31] As no lithographic patterning was used in our single step MAE process the diameters are not of uniform cross sectional shape or size (50-200 nm) but are several tens of micrometers in length.

2. Experimental

Iso-propyl-alcohol (IPA) (99.9 %), nitric acid (65 %) and hydrofluoric acid (49 %), 1-undecylenic acid (UA) (> 98 %), *N*-hydroxysuccinimide (NHS)(98 %) , *N*,*N*′-dicyclohexylcarbodiimide (DCC) (≥ 99.0 %), dichloromethane (≥ 99.8 %), ethyl acetate (≥ 99.7 %), 1,2,4-Trichlorobenzene, (+) - biotin hydrazide (98 %) were all sourced from Sigma Aldrich Ireland and used as received. 200 mm p-type silicon (100) wafers (680 micron thickness) with a resistivity of 5 – 10 Ω cm from University Wafer were used as the standard silicon substrate**.** Each wafer was cut to a size of 5 mm × 10 mm, or 10 mm^2, and cleaned with IPA before etching. Wafer coupons were sonnicated for two cycles in IPA for 20 min at 40 °C and dried under nitrogen. The substrates also had polyimide tape protecting the unpolished side during etching reactions. Substrates were immersed for a variety of times in a heated solution of 5, 10 or 12 % HF containing varying amounts of $AgNO_3$ (0.02 - 0.10 M) and maintained at 50 °C using a thermostated water bath. Ag (I) was chosen as the catalytic metal for this process as it has been reported that Ag nanoparticles bore a cylindrical hole into Si strictly along the <100> direction whereas other metals (Pt, Au) do not.[32-33] After removing the substrates from the etching bath they were washed copiously with deionized water and then treated with concentrated nitric acid to remove unwanted silver deposits. The length of the Si nanowires produced was controlled by the etching time and etchant concentration which was uniform across the entire substrate. Scanning electron microscopy (SEM) imaging was performed on a *FEI Inspect F* instrument, typically operating at an accelerating voltage of between 5 - 20 kV. Transmission electron microscopy (TEM) imaging was performed on a Jeol 2100 microscope operating at 200 kV. Prior to focused ion beam (FIB) sectioning or fluorescent imaging, the Si nanowires were removed from the carrier wafer by sonication in IPA. This IPA/ Si nanowire solution was then dropped onto a

clean Si wafer to allow the Si nanowires to lie flat on the surface. Sectioning and *in-situ* high resolution SEM imaging of the Si nanowires formed by single step MAE were carried out with an FEI Helios Nanolab Dual Beam FIB System. A protective layer of platinum was deposited over the region of interest in two stages; electron beam induced deposition was used to minimize surface damage prior to bulk deposition using the ion beam. Once deposition was completed, the FIB was used to a mill a section of a flat lying Si nanowire. After the cross section was completed the sample was then polished. Cross-sectional TEM sample preparation was performed on the flat lying Si nanowire using a standard FIB lift out technique described elsewhere [34]. All TEM images and SAED were collected on a JEOL JEM 2100F TEM operating at an accelerating voltage of 200 kV. Energy Dispersive X-Ray (EDX) analysis was performed using an Oxford instruments INCA energy system fitted to the TEM. The organic functionalisation of the nanowires was performed using a combination of procedures from the literature. *N*-Succinimidyl Undecyl-1-enate (NHS-UA) was synthesised according to the methods outlined in ref.33 and this was then chemically attached to the silicon nanowire surfaces using a thermal hydrosilation reaction carried out under inert conditions. [35] Biotin was then attached to the chemically modified nanowires using a buffer mediated procedure adapted from literature. [36] Streptavidin DyLight 650 conjugated (1 mg ml^{-1}) was diluted by 50 using phosphate buffered saline (pH 7.2) to give a stock solution. This was used to make further dilutions. 2 ml of a dilution was passed over the biotin functionalized nanowires for 30 s. The sample was then rinsed in phosphate buffered saline and dried under argon. The dye molecule excites at 652 nm and emits at the 672 nm region.

3. Results and Discussion

Varying concentrations of HF solutions, *i.e.* 5, 10 and 12 % (w/v) and Ag (I) ion concentration (0.02-0.1 M) were used to produce Si nanowires by MAE. As expected, the Si etch rate was found to increase with increasing HF concentration. [37] The anodic reaction of this electroless redox process is the dissolution of the oxidised silicon into the water soluble silicon hexafluoride anion. As silicon is the bulk material, the F^- anions are essentially the limiting reagent in this reaction. HF concentrations therefore increase the rate of the Si dissolution reaction, causing the Si to be etched at a faster rate. The corresponding cathodic reaction in this process is the reduction of Ag(I) ions to elemental Ag(0) on the surface of the Si. [38] The overall reaction can be represented by the redox type equation (1) below:

$$4Ag^+(aq) + Si(s) + 6F^-(aq) \rightarrow 4Ag(s) + 2SiF_6^{2-}(aq) \quad (1)$$

To observe any effect of changing the Ag(I) ion concentration on the morphology of the Si nanowires, experiments were undertaken using a HF concentration of 12 %, an etching time and temperature of 2 h and 50 °C respectively and a Ag(I) ion concentration between 0.02 – 0.1 M. In the same manner that increasing the HF concentration in the etching solution leads to longer Si nanowires, increasing the Ag(I) concentration should have a similar effect. [38] SEM cross sectional analysis of the samples revealed that that the mean lengths of Si nanowires increased from 80 µm to 110 µm Ag(I) ion concentrations of 0.02 M and 0.04 M respectively. However, at a Ag(I) ion concentration of 0.06 M, the mean length of the Si nanowires was measured was only 100 µm. Similarly, samples prepared with solutions containing Ag(I) ion concentrations of 0.08 and 0.1 M metal generated Si nanowires with mean length of approximately 80 µm. The shorter than expected nanowires were generally produced in etches with metal concentrations above 0.04 M. Figure 1 shows SEM images of Si nanowires generated using an etching solution containing [Ag(I)] = 0.08

M. The images show a step formed at a uniform height across the sample length and the porous nature of the nanowires formed at the step.

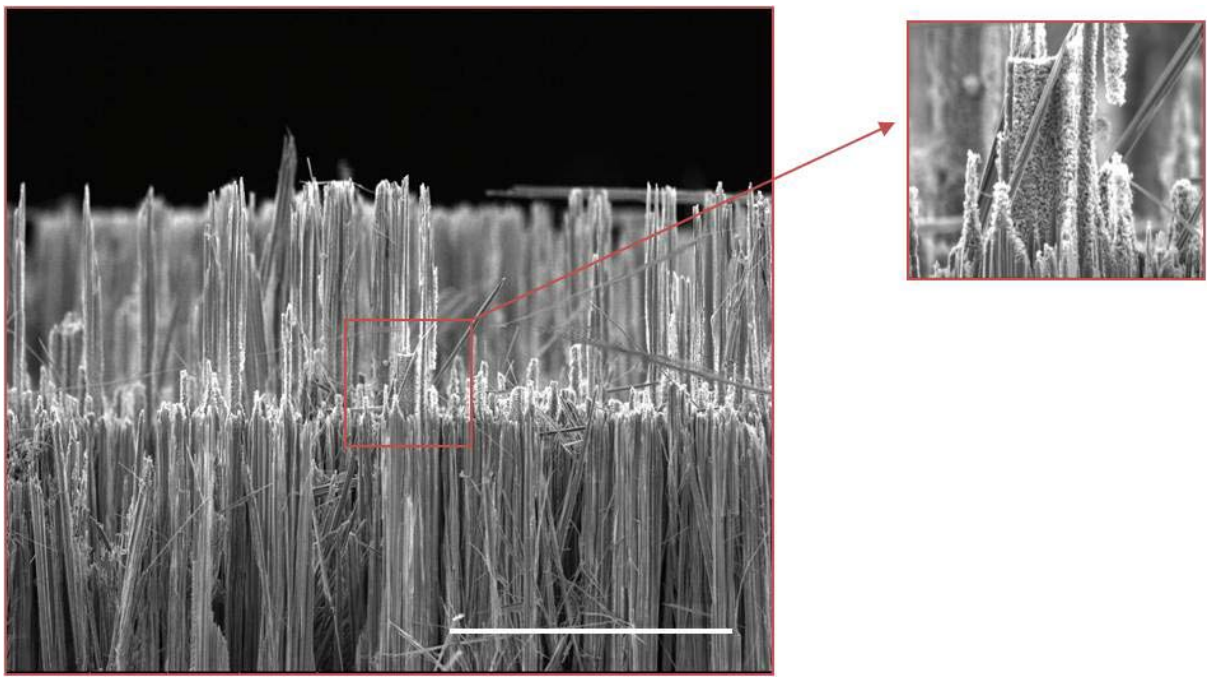

Fig. 1(Colour) SEM image of a Si substrate immersed for 2 h in an etching solution containing [$AgNO_3$] = 0.08 M and 12 % HF at a temperature of 50 °C. The Si nanowires are porous to the depth of the step. Scale bar is 30 µm.

The stepped nature of the sample can be explained by the method of sample preparation for cross sectional SEM imaging. The Si nanowires existing were so porous in nature that they simply collapsed at this weak point upon splicing of the wafer. Nanowires located elsewhere on the wafer were equally as porous but did not collapse simply because no physical strain was placed upon them, hence the "step" effect in the figure 1. A common cause for the formation of porous nanowires is high dopant concentrations (resistivity < 1 ohm cm) within the Si substrates, which can lead to crystal defects and impurities during the MAE process. [39] The dopants themselves are thought to serve as nucleation sites for pore formation by providing low energy sites for metal deposition and subsequent etching. [40] Also, highly doped Si wafers lower the barrier to charge injection across the silicon surface,

*

allowing much faster rates of etching at all exposed silicon surfaces in the etching solution. However, in our experiments Si substrates with relatively low dopant concentrations (~ 1 x 10^{15} cm^{-3}) and high resistivity (5-10 Ω cm) were used. Qu *et al.* [26] have also previously proposed that the formation of porous Si nanowires during MAE is catalysed by Ag nanoparticles resulting from the aggregation of Ag ions in solution. [26] However, the nanowires observed in this study were porous to a uniform depth indicating a change in the stoichiometric ratio of the reactants present as a function of reaction time. A deliberate change in the reactant ratio to tune the morphology of nanowires etched in the two-step fashion to form barcode nanowires has been previously reported. [29] In the one-step process described here, a change in reactant ratio occurs due to the depletion of Ag(I) ions in the etching solution, which is confirmed by the accumulation of elemental Ag dendrites on top of the Si substrates during etching. Consequently a threshold Ag(I) ion concentration must exist, which determines the balance between forming of porous or non-porous Si nanowires via the one-step etch process. Below this threshold, at Ag(I) ion concentrations below 0.04 M, non-porous wires are produced. At high Ag(I) ion concentrations, above 0.04 M, porous Si nanowires are produced. The presence of a threshold Ag(I) concentration explains why porous Si nanowires formed at the start of the etching process, when the initial Ag(I) ion concentration is above 0.04 M. During the etch process, the concentration of Ag(I) ions drops below the threshold value of 0.04 M resulting in the formation of non- porous Si nanowires wires, as observed by SEM analysis. Length control of the Si nanowires produced by the single step MAE process was quite good, when operating below this threshold initial Ag(I) concentration. Si nanowires ranging in lengths from 1.5 μm to 80 μm could easily be achieved by varying the reaction time while keeping the reaction temperature constant. Above the threshold Ag(I) concentration, this size control is no longer as predictable due to the increased porosity of the Si nanowires formed.

*

The change in morphology of the Si nanowires from porous to non-porous may also be viewed as a shift in the etching behavior from partially isotropic to mostly anisotropic. At high Ag(I) concentrations the nanowires themselves have been etched resulting in a high degree of porosity. As the Ag(I) ion reserve in the solution is depleted, this isotropic etch behavior is lessened and the etch proceeds in a more anisotropic fashion along the preferred <100> direction, with a lower degree of roughening or porisifcation. At very high Ag(I) ion concentrations ([Ag(I)] > 0.1 M) the isotropic nature of the etch is so overwhelming that no Si nanowires are produced at all and the result is a "blanket" etch of the entire wafer. A model compiled in a recent review by Huang *et al.* [38] of the two-step MAE mechanism can be adapted to explain the roughening of the Si nanowires at high metal concentrations in this one step mechanism. Firstly, Ag(I) ions close to the surface of the Si substrate capture electrons from the valence band of the Si and are deposited in the form of metallic silver nuclei [41]. One explanation for this spontaneous reduction is offered by Tong *et al.* [42] who attribute the reduction of Ag(I) to Ag(0) to the small electronegativity difference that exists between Ag (1.9) and Si (1.8). As the metal particle is reduced, the resulting holes that are generated are injected into the Si at the Ag/silicon Si interface, oxidizing the Si underneath. The concentration of holes is at a maximum at the Ag/Si interface and so etching of Si is much faster at this site than at sites with no metal coverage. At a high Ag(I) concentration, there is increased hole injection at the Ag/Si interface. The etching of the sidewalls of the nanowires occurs when the rate of hole consumption at this interface is less than the rate of hole injection. In such instances, the holes can diffuse or migrate from the injection site to the sidewalls of the pores which enables the subsequent oxidation and etching of these walls, resulting in porous nanowires being formed.

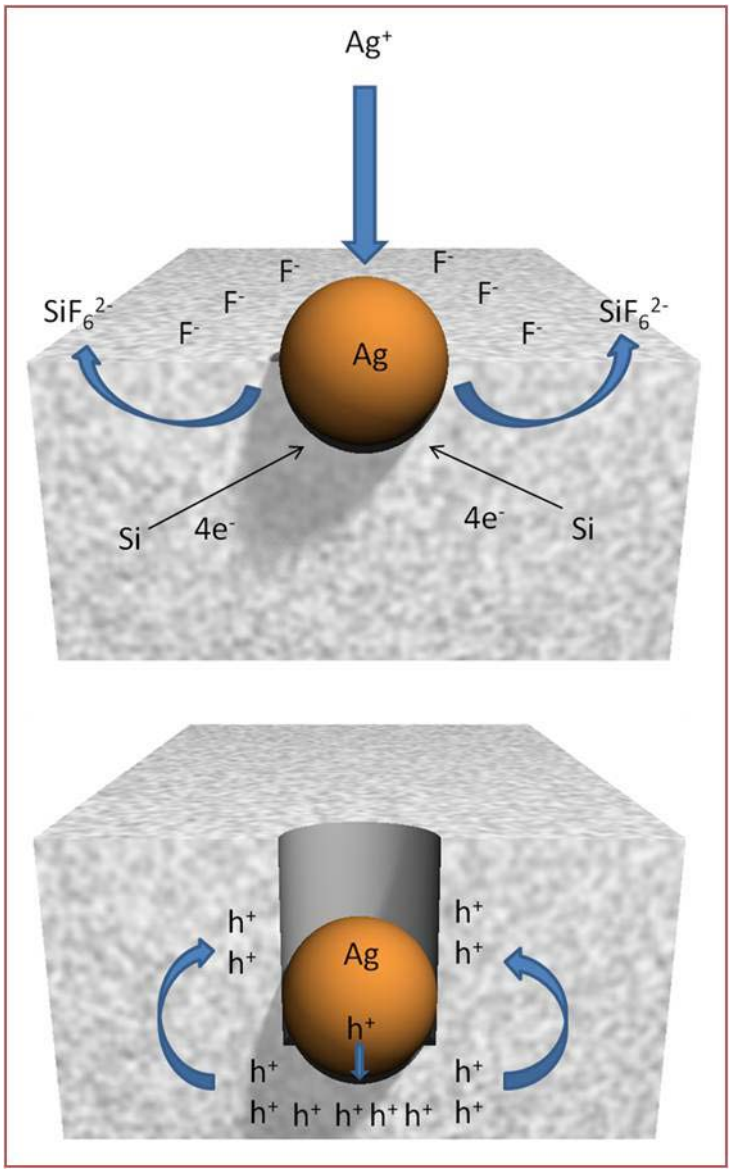

Fig. 2 (Colour) Schematic illustrating how Si nanowire porosity results from hole migration during the one-step metal assisted etching process.

A series of milder etching solutions were examined over various time scales (10, 30, 60, 90 & 120 min) to determine if isotropic etching was dominant at the beginning of the process. A 5 % HF etching solution was used instead of a 10 %, in order to establish if the Ag(I) concentration was a critical factor independent of the HF concentration. The Ag(I) ion concentration was linearly increased from 0.02 to 0.1 M. Lowly doped p-type Si wafers (< 1 x 10^{15} cm^{-3}) were immersed in etching solutions for varying amounts of time. As expected,

*

the initial blanket isotropic etch, seen in figures 3(a) and (b) gave way to an anisotropic etch over time, resulting in the generation of Si nanowires shown in figures 3(c) to (f).

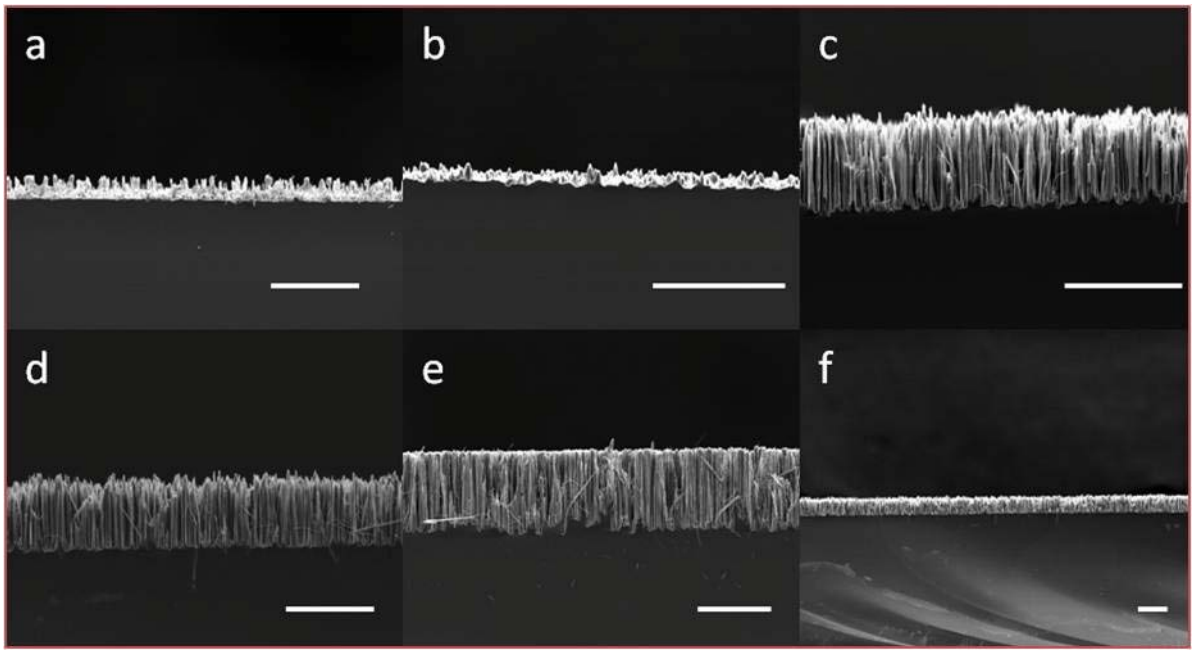

Fig. 3 (Colour) SEM images of Si substrates immersed for (a) 10 min (b) 30 min (c) 60 min (d), (f) 90 min and (e) 120 min in an etching solution containing [$AgNO_3$] = 0.04 M, 5 % HF solution at a temperature of 50 °C. All scale bars are 30 µm.

Figure 4 shows the porous nature of the silicon nanowires prepared by the one-step MAE process along with the highly crystalline plane nature of the sample by SAED.

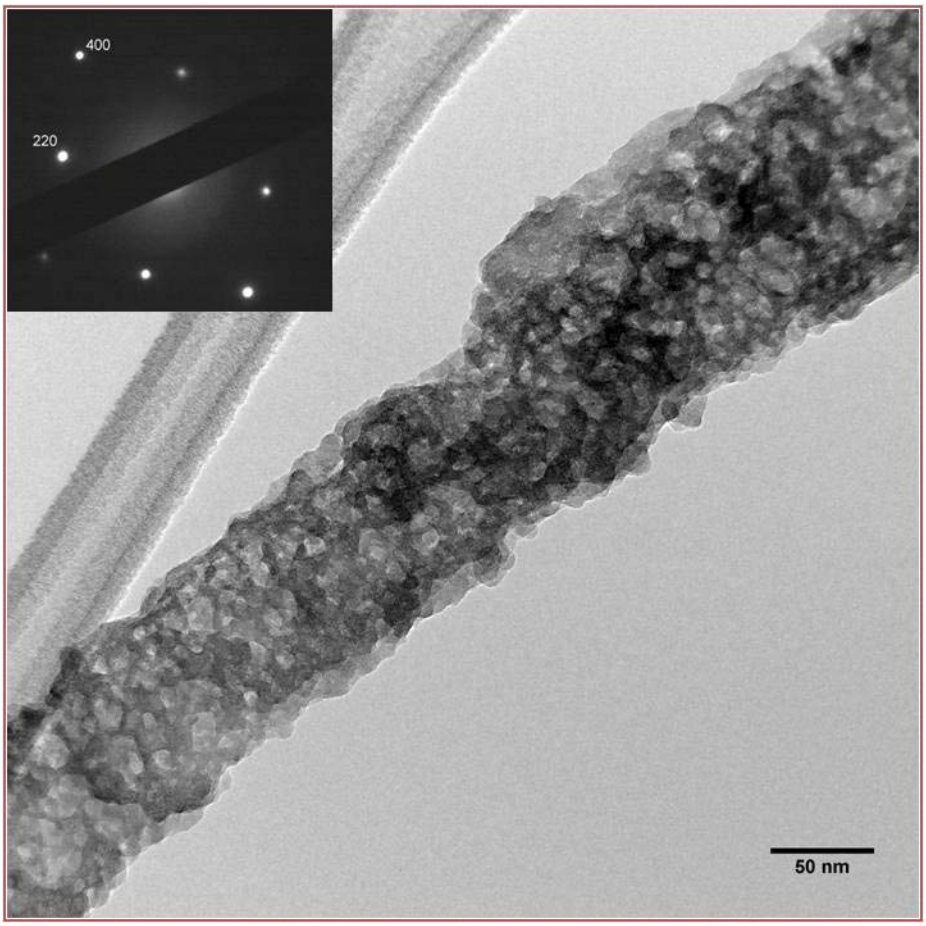

Fig. 4 (Colour) TEM image of a rough Si nanowire prepared by the one-step MAE process along with the SAED pattern (inset) showing the <100> etch direction of the wires formed.

To gain further understanding of the shift in the etch behavior from partially isotropic to anisotropic, a cross sectional study was performed on a roughened Si nanowire. The high resolution SEM images in figure 5 show that there are two distinct areas within the body of these nanowires. There is a dark black area which is the crystalline Si and the lighter grey area which is the porous, rough Si with high oxygen incorporation. EDX analysis confirmed this high oxygen content within the grey part of the Si nanowire. A line scan, moving from the outer edge of the wire to its core, showed a depleting oxygen content and the ratio of Si:O shifting from 1:2 to almost 1:0. Near the top of the nanowire, this porous area occupies a

*

significant proportion of the cross sectional area of the nanowire. However, moving down the length of the Si nanowire along the etch direction; the porous portion greatly reduces until it disappears. The gradual disappearance of the porous, oxygen rich part of the Si nanowire supports the earlier proposed mechanism of roughening by hole migration.

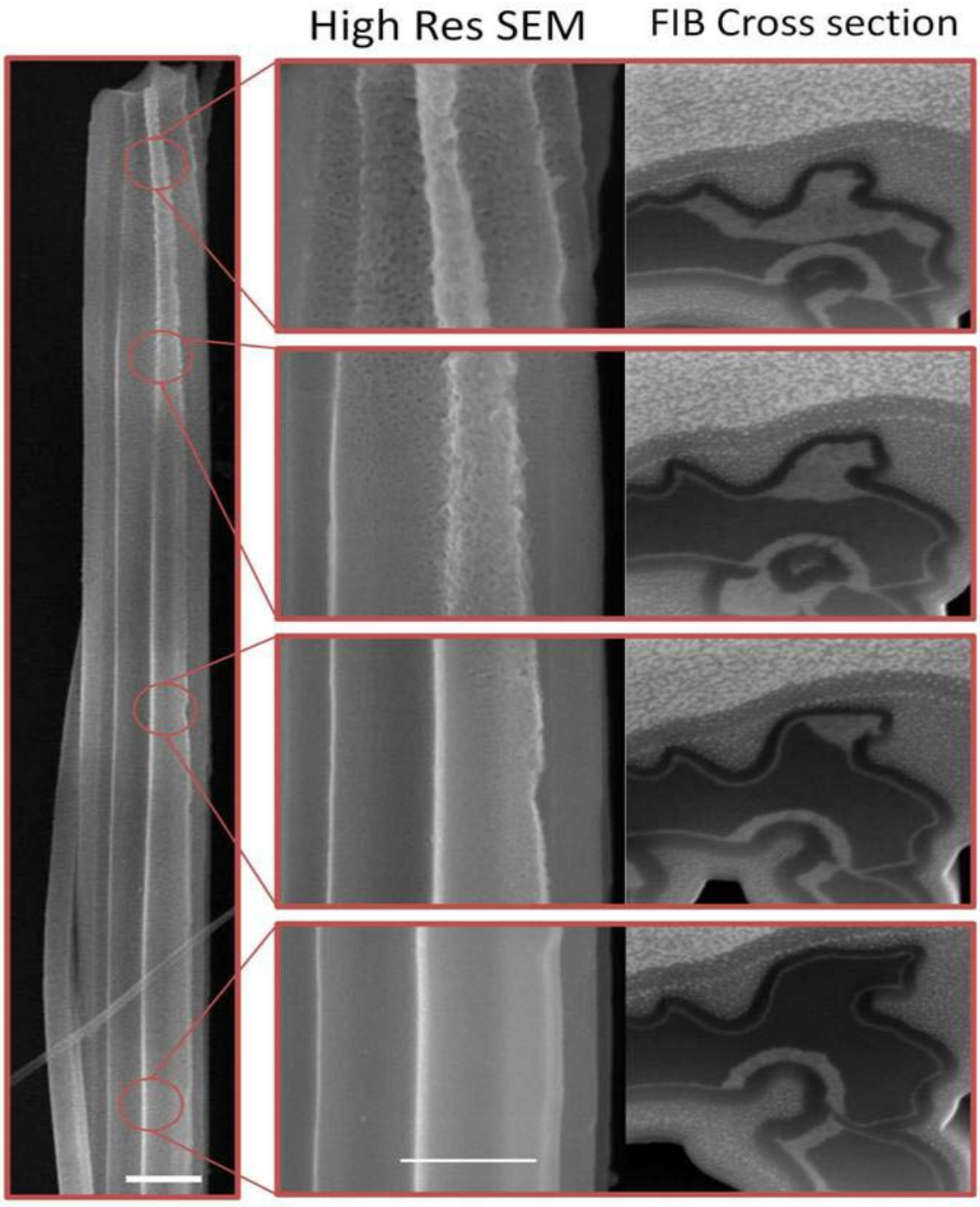

*

Fig. 5 (Colour) Left: high resolution SEM image of a MAE Si nanowire produced by the one-step process. Scale bar is 200 nm. Right: high resolution SEM plan and cross sectional view of the same Si nanowire from porous region (top) to non-porous region (bottom). (Scale bars = 200 nm)

Finally, as an exercise in application, these metal assisted etched porous wires were functionalised with biotin using a procedure modified from previous reports. [35-36] The biotin – streptavidin interaction is one of the strongest non-covalent interactions in nature. The porous section of the nanowires provides extra binding sites compared to the non-porous part and this could be potentially exploited in bio-sensing applications. After chemical modification, the nanowires were exposed to a dye conjugated streptavidin molecule. Fluorescent imaging revealed that the nanowires appeared to fluoresce more at one end of the nanowires, indicating that a greater number of dye molecules attached there.

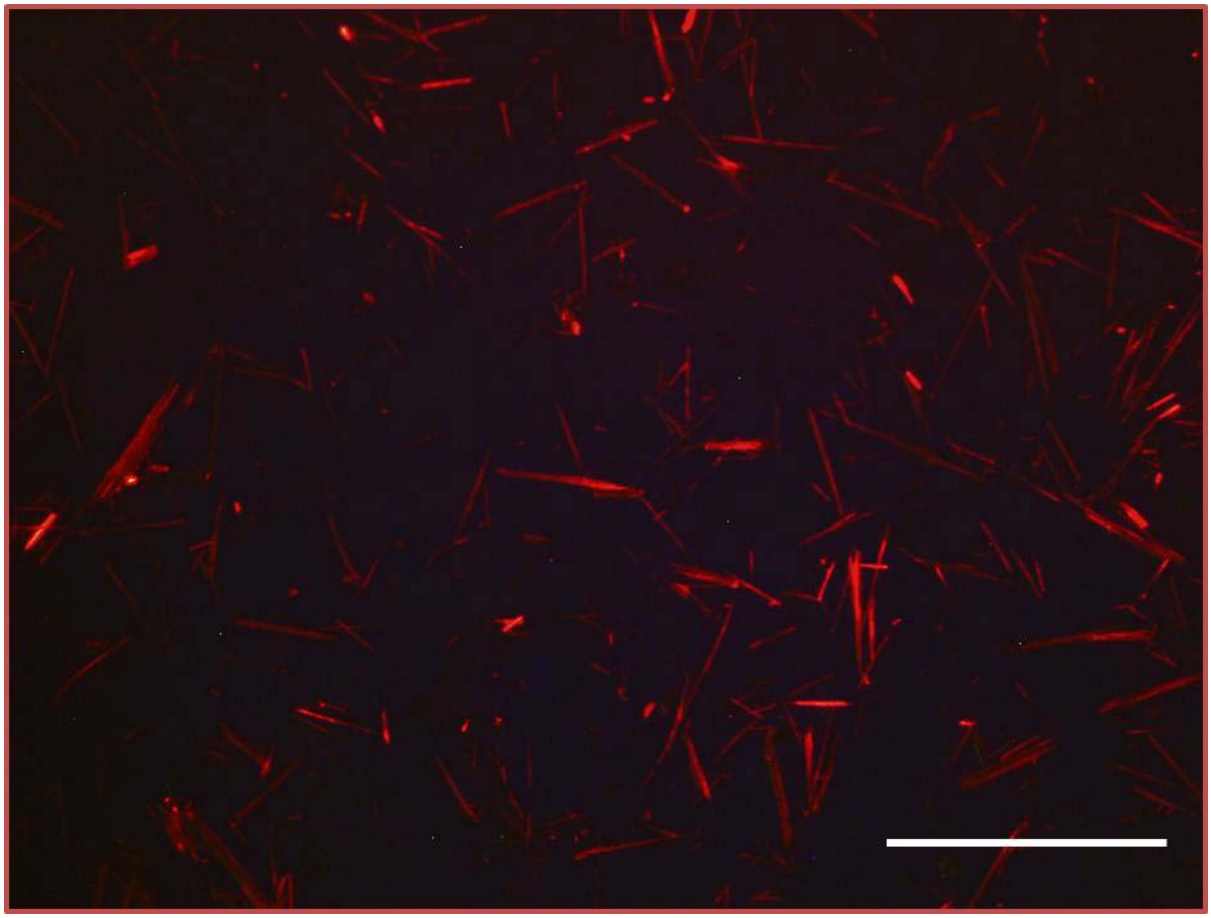

Fig. 6 (Colour) MAE Si nanowires functionalised with dye-conjugated streptavidin. The fluorescing seems to be stronger at one end of the nanowires. Scale bar is 200 nm.

4. Conclusion

The surface topography of Si nanowires formed by a one-step MAE process have been shown to depend on the initial concentration of Ag(I) ions present in the process. The control of nanowire topography, or more importantly the understanding of the nanowire roughening mechanism by MAE is an attractive goal given the role porous silicon has in the fields of energy harvesting and biosensing. Control over the porosity of densely packed arrays of Si nanowires in a one-step process eliminates the need for expensive processing and can offer

improved functionality in terms of increased surface area and higher anti-reflective characteristics. The concentration of Ag(I) ions and the immersion time of the substrate in the etchant solution significantly affects the uniformity and porosity of the Si generated, even without the use of an external oxidant as in a two-step process. The change from isotropic to anisotropic etching, as determined by cross-sectional SEM and TEM imaging, highlights the impact of the metal ion concentration on the mechanism of nanowire roughening by hole migration.

Acknowledgements

The research leading to these results has received funding from the EU 7th Framework Programme under the SiNAPS project (Grant: 257856).

References

1. Y. Cui and C. M. Lieber: Science. **291** (2001) 851.
2. M. S. Gudiksen, L. J. Lauhon, J. Wang, D. C. Smith and C. M. Lieber: Nature. **415** (2002) 617.
3. M. C. McAlpine, R. S. Friedman and C. M. Lieber: Proceedings of the Ieee. **93** (2005) 1357.
4. G. F. Zheng, W. Lu, S. Jin and C. M. Lieber: Adv. Mater. **16** (2004) 1890.
5. A. Javey, S. Nam, R. S. Friedman, H. Yan and C. M. Lieber: Nano Lett. **7** (2007) 773.
6. N. Singh, A. Agarwal, L. K. Bera, T. Y. Liow, R. Yang, S. C. Rustagi, C. H. Tung, R. Kumar, G. Q. Lo, N. Balasubramanian and D. L. Kwong: IEEE Electron Device Lett. **27** (2006) 383.
7. K. Hagedorn, C. Forgacs, S. Collins and S. Maldonado: J. Phys. Chem. C. **114** (2010) 12010.
8. W. Chern, K. Hsu, I. S. Chun, B. P. de Azeredo, N. Ahmed, K. H. Kim, J. M. Zuo, N. Fang, P. Ferreira and X. L. Li: Nano Lett. **10** (2010) 1582.
9. B. Z. Tian, X. L. Zheng, T. J. Kempa, Y. Fang, N. F. Yu, G. H. Yu, J. L. Huang and C. M. Lieber: Nature. **449** (2007) 885.
10. Y. Y. Wu, R. Fan and P. D. Yang: Nano Lett. **2** (2002) 83.
11. D. D. D. Ma, C. S. Lee, F. C. K. Au, S. Y. Tong and S. T. Lee: Science. **299** (2003) 1874.
12. N. Wang, Y. H. Tang, Y. F. Zhang, C. S. Lee, I. Bello and S. T. Lee: Chem. Phys. Lett. **299** (1999) 237.
13. N. Wang, Y. H. Tang, Y. F. Zhang, C. S. Lee and S. T. Lee: Physical Review B. **58** (1998) 16024.
14. A. I. Hochbaum, R. Fan, R. R. He and P. D. Yang: Nano Lett. **5** (2005) 457.
15. Y. W. Wang, V. Schmidt, S. Senz and U. Gosele: Nat. Nanotechnol. **1** (2006) 186.
16. T. Hanrath and B. A. Korgel: Adv. Mater. **15** (2003) 437.
17. J. D. Holmes, K. P. Johnston, R. C. Doty and B. A. Korgel: Science. **287** (2000) 1471.
18. N. Wang, Y. Cai and R. Q. Zhang: Materials Science & Engineering R-Reports. **60** (2008) 1.
19. S. Barth, F. Hernandez-Ramirez, J. D. Holmes and A. Romano-Rodriguez: Prog. Mater Sci. **55** (2010) 563.
20. J. Kim, H. Han, Y. H. Kim, S. H. Choi, J. C. Kim and W. Lee: Acs Nano. **5** (2011) 3222.
21. S. W. Chang, V. P. Chuang, S. T. Boles, C. A. Ross and C. V. Thompson: Adv. Funct. Mater. **19** (2009) 2495.
22. Z. P. Huang, X. X. Zhang, M. Reiche, L. F. Liu, W. Lee, T. Shimizu, S. Senz and U. Gosele: Nano Lett. **8** (2008) 3046.
23. L. Boarino, D. Imbraguglio, E. Enrico, N. De Leo, F. Celegato, P. Tiberto, N. Pugno and G. Amato: Physica Status Solidi a-Applications and Materials Science. **208** (2011) 1412.
24. G. B. Jia, M. Steglich, I. Sill and F. Falk: Sol. Energy Mater. Sol. Cells. **96** (2012) 226.

*

25. A. I. Hochbaum, R. K. Chen, R. D. Delgado, W. J. Liang, E. C. Garnett, M. Najarian, A. Majumdar and P. D. Yang: Nature. **451** (2008) 163.

26. Y. Q. Qu, L. Liao, Y. J. Li, H. Zhang, Y. Huang and X. F. Duan: Nano Lett. **9** (2009) 4539.

27. X. L. Wang and W. Q. Han: Acs Applied Materials & Interfaces. **2** (2010) 3709.

28. H. Kim, B. Han, J. Choo and J. Cho: Angew. Chem.-Int. Edit. **47** (2008) 10151.

29. C. Chiappini, X. Liu, J. R. Fakhoury and M. Ferrari: Adv. Funct. Mater. **20** (2010) 2231.

30. H. Chen, R. Zou, H. Chen, N. Wang, Y. Sun, Q. Tian, J. Wu, Z. Chen and J. Hu: J. Mater. Chem. **21** (2011) 801.

31. M. L. Zhang, K. Q. Peng, X. Fan, J. S. Jie, R. Q. Zhang, S. T. Lee and N. B. Wong: J. Phys. Chem. C. **112** (2008) 4444.

32. K. Tsujino and M. Matsumura: Adv. Mater. **17** (2005) 1045.

33. C. L. Lee, K. Tsujino, Y. Kanda, S. Ikeda and M. Matsumura: J. Mater. Chem. **18** (2008) 1015.

34. L. A. Giannuzzi and F. A. Stevie: Micron. **30** (1999) 197.

35. J. Macossay, S. A. Shamsi and I. M. Warner: Tetrahedron Lett. **40** (1999) 577.

36. M. Yang, R. L. M. Teeuwen, M. Giesbers, J. Baggerman, A. Arafat, F. A. de Wolf, J. C. M. van Hest and H. Zuilhof: Langmuir. **24** (2008) 7931.

37. K. Peng, A. Lu, R. Zhang and S. T. Lee: Adv. Funct. Mater. **18** (2008) 3026.

38. Z. P. Huang, N. Geyer, P. Werner, J. de Boor and U. Gosele: Adv. Mater. **23** (2011) 285.

39. S. Cruz, A. Honig-dOrville and J. Muller: J. Electrochem. Soc. **152** (2005) C418.

40. A. I. Hochbaum, D. Gargas, Y. J. Hwang and P. Yang: Nano Lett. **9** (2009) 3550.

41. K. Q. Peng, Y. Wu, H. Fang, X. Y. Zhong, Y. Xu and J. Zhu: Angew. Chem.-Int. Edit. **44** (2005) 2737.

42. H. Tong, C. M. Wang, W. C. Ye, Y. L. Chang and H. L. Li: Chin. J. Chem . **25** (2007) 208.